Nanoindentation into a metastable austenite triggers the martensitic phase transformation—An atomistic study

Cite as: AIP Advances **9**, 015228 (2019); https://doi.org/10.1063/1.5081496
Submitted: 15 November 2018 . Accepted: 16 January 2019 . Published Online: 29 January 2019

Jerome Meiser, Iyad Alabd Alhafez, Tilmann Beck, Marek Smaga, Ralf Müller, and Herbert M. Urbassek

Nanoindentation into a metastable austenite triggers the martensitic phase transformation—An atomistic study

Cite as: AIP Advances 9, 015228 (2019); doi: 10.1063/1.5081496
Submitted: 15 November 2018 • Accepted: 16 January 2019 •
Published Online: 29 January 2019

View Online Export Citation CrossMark

Jerome Meiser,[1] Iyad Alabd Alhafez,[1] Tilmann Beck,[2] Marek Smaga,[2] Ralf Müller,[2] and Herbert M. Urbassek[1,a)]

AFFILIATIONS

[1]Physics Department and Research Center OPTIMAS, University Kaiserslautern, Erwin-Schrödinger-Straße, D-67663 Kaiserslautern, Germany

[2]Department of Mechanical and Process Engineering, University Kaiserslautern, Erwin-Schrödinger-Straße, D-67663 Kaiserslautern, Germany

[a)]**Electronic address:** urbassek@rhrk.uni-kl.de; URL: http://www.physik.uni-kl.de/urbassek/

ABSTRACT

Indentation into a metastable austenite may induce the phase transformation to the bcc phase. We study this process using atomistic simulation. At temperatures low compared to the equilibrium transformation temperature, the indentation triggers the transformation of the entire crystallite: after starting the transformation, it rapidly proceeds throughout the simulation crystallite. The microstructure of the transformed sample is characterized by twinned grains. At higher temperatures, around the equilibrium transformation temperature, the crystal transforms only locally, in the vicinity of the indent pit. In addition, the indenter produces dislocation plasticity in the remaining austenite. At intermediate temperatures, the crystal continuously transforms throughout the indentation process.

I. INTRODUCTION

Conventional austenitic stainless steels and new TRIP (TRansformation Induced Plasticity) steels are metastable at temperatures below the martensite deformation temperature and can transform from the fcc austenite phase to the hcp ϵ or/and to the bcc α martensite phase during mechanical loading.[1,2] This transformation induces significant changes in the mechanical properties of the materials, e.g., an increase in strength;[3] also their physical properties, e.g., a change from the paramagnetic to the ferromagnetic state,[4] and their technological properties are affected, e.g., an increase in wear resistance.[5] The formation of bcc martensite depends on various factors, such as temperature, plastic deformation, grain orientation, deformation rate, etc., and it is difficult to study all these parameters experimentally. However, atomistic simulation allows to study the influence of these factors on bcc martensite formation using molecular dynamics (MD) simulation. In addition, MD simulations can be used to provide basic information about the transformation process to mesoscopic material models such as phase field models, see for example Refs. 6–8.

Previous experiments found that local mechanical loading – such as under nanoindentation – can induce the transformation of the metastable austenitic phase. Kim *et al.*[9] observed that several martensitic variants are locally formed under indentation such that the external stress is best accommodated. Roa *et al.*[10,11] observed the formation of martensite in a region of lenticular shape around the imprint. In later work, these authors also studied the fatigue behavior under cyclic loading of metastable austenites.[12]

In the present paper, we study the phase transformation of a metastable austenite under nanoindentation using MD simulation. We can monitor the evolution of the $\gamma \rightarrow \alpha$ transformation as a function of the temperature at which the indentation is performed. As a result,

we find a systematic change from a localized to a global (i.e., grain-spanning) transformation with decreasing temperature.

II. SIMULATION METHOD

We use classical MD simulations to study the indentation of a pure Fe crystal. The crystal has an fcc lattice structure with a $(001)_{fcc}$ surface. Fig. 1 provides a schematic view of the simulation system. The x, y, and z directions correspond to the $[100]_{fcc}$, $[010]_{fcc}$, and $[001]_{fcc}$ crystal orientations. The sample contains 4608000 atoms and and has a size of approximately 439 Å × 439 Å × 293 Å. Fe atoms interact via the Meyer-Entel potential.[13]

Two atom layers at the bottom of the crystal are fixed to prevent any rigid-body motion of the substrate. The next four layers at the bottom and the outermost four layers at the sample sides are held at a fixed temperature T. We perform simulations for a variety of temperatures between 0 and 550 K. Periodic boundary conditions are employed in x and y direction.

The indenter is modeled as a rigid sphere with a radius of R = 50 Å and we indent until a depth of 50 Å with a velocity of 20 m/s. It interacts with the Fe atoms via a potential[14]

$$V(r) = k(R - r)^3, \quad r < R, \tag{1}$$

where the indenter stiffness has been set to $k = 10$ eV/Å^3.[14,15]

We prepare the systems by heating an fcc-Fe crystal to the intended temperature and relaxing it for 50 ps. The crystals are initially defect-free.

We use adaptive common-neighbor analysis[16–18] to identify the local crystal structures, and DXA[19] to analyze the dislocations formed during indentation. These algorithms as well as the rendering of the snapshots are provided by OVITO.[20]

A. Meyer-Entel potential

We use the Meyer-Entel potential[13] to describe the interaction in Fe, since it is able to implement the bcc-fcc phase transformation in Fe. It should be mentioned that among the many potentials available to model Fe, there are only very few that implement the α–γ transformation.[22] Among these, the Meyer-Entel potential is the one employed most often and studied best.[23,24] The equilibrium transition temperature T_c of this potential amounts to 550 ± 50 K, as it was determined by both free-energy calculations[22,25] and dynamic molecular dynamics simulations.[21,26] In reality, this temperature is at 1184 K; this means that the temperature dependence of the results presented here needs be scaled appropriately to apply to realistic systems.

The martensitic transformation is initiated upon cooling a crystal from a high-temperature fcc state. This transformation does not occur at T_c, but is kinetically hindered. We demonstrate this feature by displaying in Fig. 2 the evolution of the free-energy between the fcc and the bcc phase when transforming an fcc crystal to a bcc crystal via a Bain path;[21] the evolution along a Nishiyama-Wassermann path is very similar.[21] The free energy has been evaluated from the work done under the transformation using the metric-scaling technique[22,27] as in Ref. 21. Both fcc and bcc are local minima of the free energy indicating their (meta)stability. Indeed, upon increasing the temperature, the global minimum shifts from bcc to fcc. Most interesting is the kinetic barrier to transformation; for a metastable fcc crystal it increases with temperature indicating that the martensitic transition is more strongly impeded at high than at low temperatures, in agreement with experiment.

In the Meyer-Entel potential, it has been found that for a bulk crystal, the martensitic transformation temperature depends on the size of the simulation crystallite.[28] In addition, the transformation is eased if open volume is available – in the form of point defects[13] or surfaces[29] – to allow atoms to change their positions freely.

A drawback of the Meyer-Entel potential is that the atomic volumes Ω in the fcc phase is not correctly reproduced. In fact the Meyer-Entel potential predicts the fcc phase (Ω = 12.57 Å^3) to have a larger volume than the bcc phase (12.26 Å^3), while in experiment the bcc phase (11.77 Å^3) is more open than the fcc phase (11.38 Å^3);[28,30] here data at 300 K have been reported.[31] As Pepperhof and Acet[30] note, it is common that the more stable phase has a smaller volume; while Fe

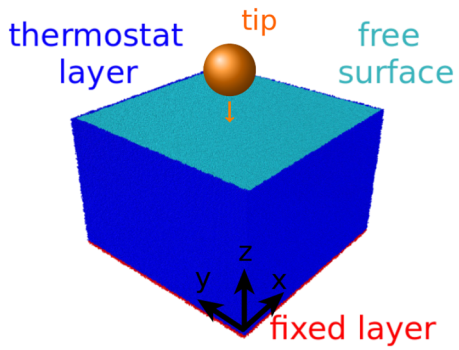

FIG. 1. Schematics of the simulation setup showing the indenter tip above the substrate. The free top surface, the bottom fixed layer, the boundary thermostat layers, and the orientation of the cartesian axes are indicated.

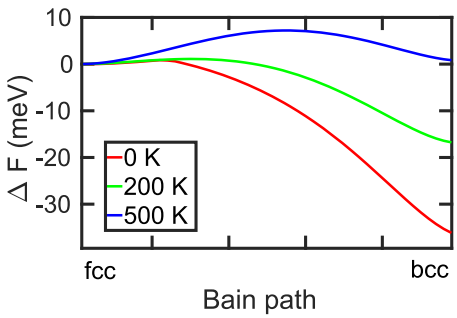

FIG. 2. Evolution of the free-energy difference between the fcc and the bcc phase along the Bain path for various temperatures.[21]

contradicts this rule, it explains why the interaction potential used in MD sticks to it. However, it has been found[32] that the nucleation kinetics and growth of the martensite phase at an fcc grain boundary is correctly reproduced in the Ackland potential[33] that similar to ours predicts a volume decrease upon the martensitic transformation; this argument has been used in favor of the Meyer-Entel potential as well.[34] We extend this argument here by arguing that phase nucleation at a free surface and induced by the indentation will be affected equally little by this feature.

Planar defects such as stacking faults are implemented well in the fcc phase of Meyer-Entel iron.[34] Also dislocations are modeled qualitatively correctly in the fcc phase; this can be observed by comparing the value of the stacking-fault energy – which is key to determining the dislocation dissociation – in the Meyer-Entel potential (–54 meV/m^2)[34] with ab-initio data for paramagnetic fcc-Fe (–105 meV/m^2).[35]

III. RESULTS

A. Synopsis

Fig. 3 provides an overview of the phase transformation induced by the indentation process.

- At low temperatures, $T \leq 140$ K, the indentation triggers a phase transformation which spans more or less the entire simulation crystallite.
- At intermediate temperatures, up to around 200 K, martensite needles are formed stretching far out in ⟨110⟩ direction.
- At even higher temperature, up to 350 K, only the local volume around the indent pit transforms.
- Finally, at still higher temperatures, the indentation is not able to trigger any substantial amount of transformation, even though the temperatures are still below the equilibrium transformation temperature.

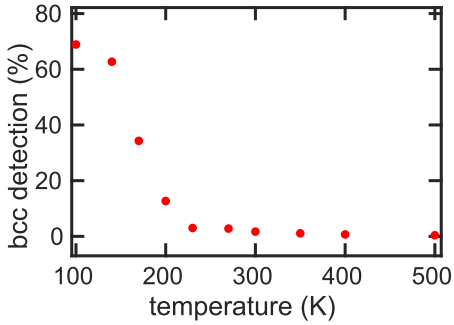

FIG. 4. Percentage of bcc atoms detected at the end of the indentation as a function of the temperature.

Fig. 4 summarizes these findings by plotting the fraction of Fe atoms transformed by the indentation process as a function of temperature. The most prominent feature is the sharp decrease of martensite formation in a small temperature window of around 150–200 K.

In the following we will discuss the microstructures formed in an exemplary way for 100, 200 and 500 K.

B. 100 K

The process of the indentation at 100 K is shown in Fig. 5a with the help of a force-penetration curve. Similar results were observed at all temperatures below 130 K. After an initial phase, the material starts transforming between 10 and 15 Å indentation depth, and already at 20 Å, the material is almost entirely transformed. Austenite remains at the bottom of the

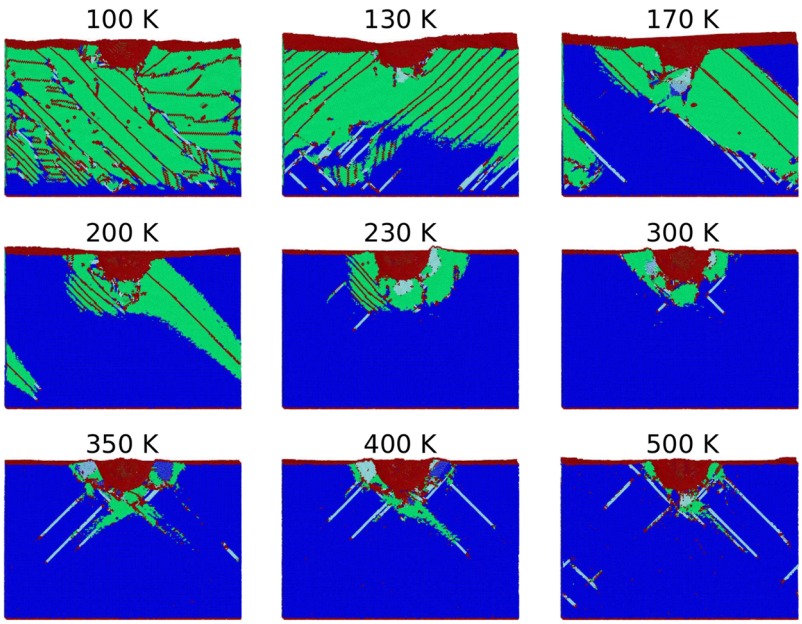

FIG. 3. Synopsis over the transformation process induced by the indentation at the various temperatures studied. The colors denote the local crystal structure: green: bcc; dark blue: fcc; light blue: hcp; red: unknown.

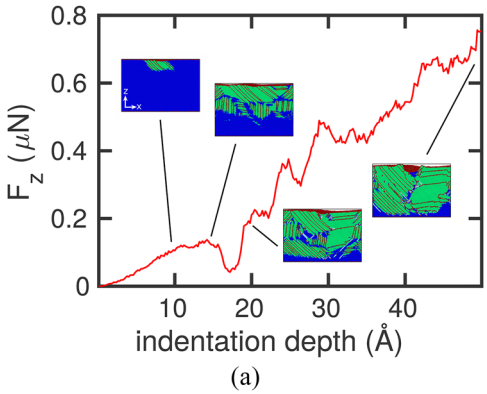

(a)

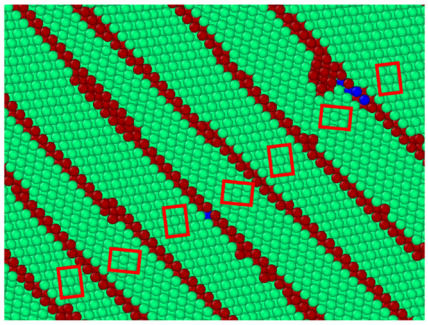

(b)

FIG. 5. (a) Dependence of the indentation force, F_z, on the indentation depth at temperature 100 K; snapshots visualize the evolution of microstructure during indentation. (b) Zoom into the snapshot at 50 Å indentation depth – viewed in the *x*-*z* plane – displaying the twinned martensitic microstructure highlighted by the red rectangles. Colors denote local lattice structures as in Fig. 3.

sample; there it is stabilized by the boundaries applied, viz. the fixed atom layer.

The indentation force, F_z, displays a minimum at around 17 Å indentation depth. It is caused by the shrinkage of the material during the ongoing martensitic transformation, as during the martensitic phase transition the volume of the sample becomes slightly reduced,[36,37] see also Sect. II A. Similar results were obtained during an experimental nanoindentation in metastable TRIP steel with the Mn-Al-Si alloying concept.[9]

Fig. 5b highlights the microstructure formed, which consists of an array of twin boundaries. The twin boundaries are $(112)_{bcc}$ planes; in the cut shown in Fig. 5b, they run in a $[\bar{1}01]_{fcc}$ direction, corresponding to a $\langle 111\rangle_{bcc}$ direction in the transformed material.

C. 200 K

Indentation at higher temperature does no longer induce a volume spanning transformation of the austenite. Particularly interesting are the phenomena occurring in the temperature range of 170 – 200 K, where the fraction of transformed material decreases to 10–30 %, see Fig. 4.

The indentation process at a temperature of 200 K is shown in Fig. 6a. Here the new phase grows continuously with proceeding indentation. While the phase transformation process is now more strongly localized around the indentation point, still fingers of the martensitic phase – marked as '1' and '2' in Fig. 6b – expand in two diagonal directions. An inspection of the crystallography involved shows that bcc grain 2 grows in $[101]_{fcc}$ direction, corresponding to the diagonal of the *x*–*z* plane, see Fig. 6c, while bcc grain 1 grows in $[011]_{fcc}$ direction, the diagonal of the *y*–*z* plane. This becomes particularly clear in Fig. 6c, which shows grain 2 in a close-up view. The diagonal here is the $[01\bar{1}]_{fcc}$ direction, which transforms to a $\langle 111\rangle_{bcc}$ direction in the phase-changed material. Here, in contrast to the fully transformed materials visualized in Fig. 5b for 100 K, only a single twin boundary is formed.

The indenter force necessary to penetrate to maximum depth (50 Å) amounts to 0.55 μN. This is considerably less than in the 100 K indent, Fig. 5, where 0.75 μN were needed. Also in the case of the 500 K indent to be discussed below, the maximum force is large, 0.70 μN. At both 100 K and 500 K, the indentation proceeds essentially in a single-phase material, viz. bcc and fcc, respectively, while for 200 K, the material continuously keeps transforming under the indentation. As the material shrinks for the Meyer-Entel potential, less force is needed in this case. We note that the initial steepness of the force-indentation curve is smallest for the 100 K case, where – due to the shrinkage of the material while transforming under the Meyer-Entel potential – the phase transformation reduces the force needed to indent.

In the vicinity of the martensitic phase, the remaining austenite phase is plastically deformed by the indentation process. This is highlighted in Fig. 6b by the dislocation lines shown. Some of them are decorated by bcc material; this follows common knowledge that dislocations can act as nucleation centers for the transformation.[38,39]

D. 500 K

The process of the indentation at a temperature of 500 K is shown in Fig. 7a. The energy barrier for the phase transition is here already high, see Fig. 2. For temperatures above 200 K we observe almost no phase transformation, as less than 2 % of all atoms are detected as bcc (Fig. 4). Only small areas around the indentation center are transformed into bcc. There the stress acting on the sample is highest.

At 500 K, only 0.4 % of the material is transformed. The bcc phase is strongly localized around the indenter tip, but forms no homogeneous region. Rather it has a very irregular shape, and follows the dislocation lines forming in the remaining austenite. It is known that dislocations can act as nucleation centers for the transformation.[38,39]

A dense network of dislocations forms in the austenite phase, such as it is commonly observed in MD studies of indentation into fcc metals.[40,41] The evolution of this network can be followed in the snapshots shown in Fig. 7a. Besides a dense zone surrounding the indenter tip, the emission of prismatic loops is observed. We conclude that at

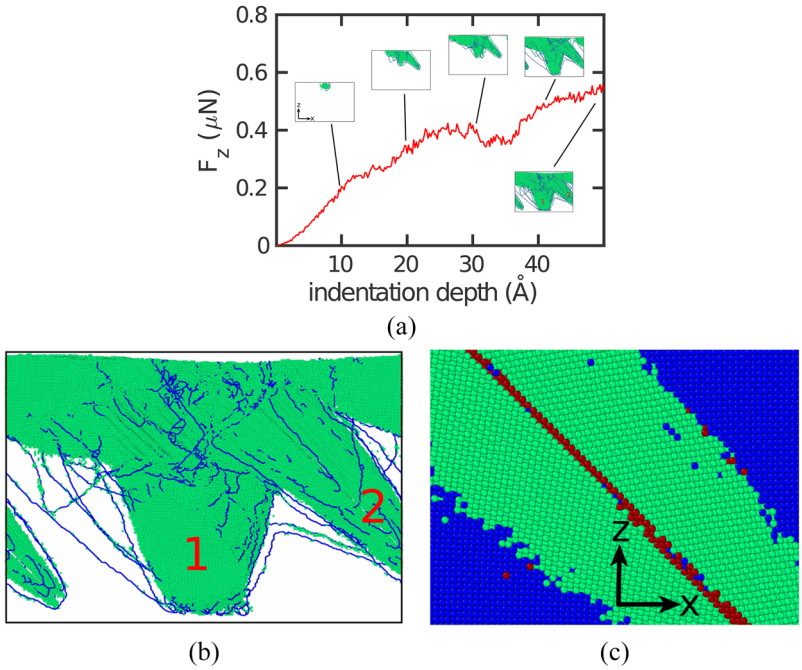

FIG. 6. (a) Similar to Fig. 5a, but for 200 K. (b) Zoom into the snapshot at 50 Å indentation depth; two martensitic grains are marked as '1' and '2'. Green colors denote the transformed bcc material; blue lines denote dislocations in the remaining fcc phase. (c) Detailed view into the atomistic structure of bcc grain 2 showing a twin boundary; colors as in Fig. 3.

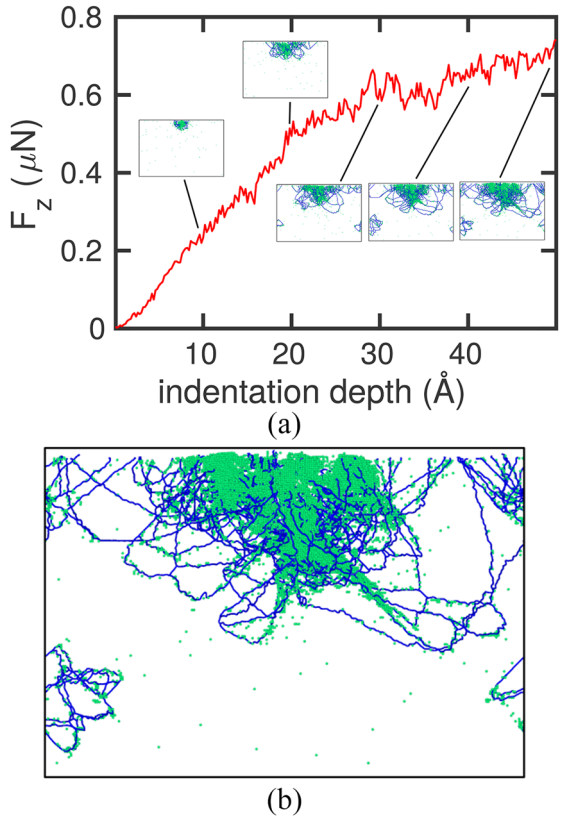

FIG. 7. (a) Similar to Figs. 5 and 6, but for 500 K. (b) Snapshot at 50 Å indentation depth; colors as in Fig. 6.

500 K, the metal prefers to react to the indentation by generating dislocations rather than by inducing the phase transformation.

IV. SUMMARY

Our main findings are:

1. Indentation into a metastable austenite may induce the phase transformation to the bcc phase.
2. At low temperatures, the indentation acts as a sudden trigger; after starting the transformation it rapidly proceeds throughout the simulation crystallite. The microstructure of the transformed sample is characterized by twinned grains.
3. At high temperatures, around the transformation temperature T_c, the crystal transforms only locally, in the vicinity of the indent pit. In addition, the indenter produces dislocation plasticity in the remaining austenite.
4. At intermediate temperatures, the crystal continuously transforms throughout the indentation process.

ACKNOWLEDGMENTS

We acknowledge support by the Deutsche Forschungsgemeinschaft via the Sonderforschungsbereich 926, project number 172116086. Access to the computational resources provided by the compute cluster 'Elwetritsch' of the University of Kaiserslautern is appreciated.

This is a theoretical study that does not use or create new data other than can be reproduced with the information contained in the method section of the paper.

REFERENCES

[1] J. K. L. Lai, K. H. Lo, and C. H. Shek, eds., *Stainless steels: an introduction and their recent developments* (Bentham Science Publishers, 2012).
[2] S. Ackermann, S. Martin, M. R. Schwarz, C. Schimpf, D. Kulawinski, C. Lathe, S. Henkel, D. Rafaja, H. Biermann, and A. Weidner, Metal. Mat. Trans. A **47A**, 95 (2016).
[3] M. Smaga, F. Walther, and D. Eifler, Mater. Sci. Eng. A **483-484**, 394 (2008).
[4] M. Smaga and D. Eifler, MP Materials Testing **51**, 370 (2009).
[5] D. Frölich, B. Magyar, B. Sauer, P. Mayer, B. Kirsch, J. Aurich, R. Skorupski, M. Smaga, T. Beck, and D. Eifler, Wear **328-329**, 123 (2015).
[6] R. Schmitt, R. Müller, C. Kuhn, and H. M. Urbassek, Arch. Appl. Mech. **83**, 849 (2013).
[7] R. Schmitt, B. Wang, H. M. Urbassek, and R. Müller, Techn. Mech. **33**, 119 (2013).
[8] S. Schmidt, C. Plate, R. Müller, R. Müller, J. Meiser, and H. M. Urbassek, Proc. Appl. Math. Mech. **16**, 481 (2016).
[9] Y. Kim, T.-H. Ahn, D.-W. Suh, and H. N. Hana, Scripta Materialia **104**, 13 (2015).
[10] J. J. Roa, G. Fargas, A. Mateo, and E. Jimenez-Pique, Materials Science and Engineering: A **645**, 188 (2015).
[11] I. Sapezanskaia, J. J. Roa, G. Fargas, M. Turon-Vinas, T. Trifonov, R. K. Njiwa, A. Redjaimia, and A. Mateo, Materials Characterization **131**, 253 (2017).
[12] J. J. Roa, I. Sapezanskaia, G. Fargas, R. Kouitat, A. Redjaimia, and A. Mateo, Materials Science and Engineering: A **713**, 287 (2018).
[13] R. Meyer and P. Entel, Phys. Rev. B **57**, 5140 (1998).
[14] C. L. Kelchner, S. J. Plimpton, and J. C. Hamilton, Phys. Rev. B **58**, 11085 (1998).
[15] G. Ziegenhain, A. Hartmaier, and H. M. Urbassek, J. Mech. Phys. Sol. **57**, 1514 (2009).
[16] J. D. Honeycutt and H. C. Andersen, J. Phys. Chem. **91**, 4950 (1987).
[17] A. S. Clarke and H. Jonsson, Phys. Rev. B **47**, 3975 (1993).
[18] D. Faken and H. Jonsson, Comput. Mater. Sci. **2**, 279 (1994).
[19] A. Stukowski and K. Albe, Model. Simul. Mater. Sci. Eng. **18**, 085001 (2010).
[20] A. Stukowski, Model. Simul. Mater. Sci. Eng. **18**, 015012 (2010), http://www.ovito.org/.
[21] L. Sandoval, H. M. Urbassek, and P. Entel, New J. Phys. **11**, 103027 (2009).
[22] C. Engin, L. Sandoval, and H. M. Urbassek, Model. Simul. Mater. Sci. Eng. **16**, 035005 (2008).
[23] H. M. Urbassek and L. Sandoval, in *Phase transformations in steels*, edited by E. Pereloma and D. V. Edmonds (Woodhead Publishing Limited, Cambridge, UK, 2012), vol. 2: Diffusionless transformations, high strength steels, modelling and advanced analytical techniques, pp. 433–463.
[24] X. Ou, Materials Science and Technology **33**, 822 (2017).
[25] L. Sandoval and H. M. Urbassek, Nano Lett. **9**, 2290 (2009).
[26] L. Sandoval, H. M. Urbassek, and P. Entel, Phys. Rev. B **80**, 214108 (2009).
[27] M. A. Miller and W. P. Reinhardt, J. Chem. Phys. **113**, 7035 (2000).
[28] E. Sak-Saracino and H. M. Urbassek, Eur. Phys. J. B **88**, 169 (2015).
[29] B. Wang and H. M. Urbassek, Metall. Mater. Trans. A **47**, 2471 (2016).
[30] W. Pepperhoff and M. Acet, *Constitution and Magnetism of Iron and its Alloys* (Springer, Berlin, 2001).
[31] In Ref. 28, the lattice constants calculated for the Meyer-Entel potential in Table 1 apply to 0 K, and not to 300 K, as wrongly stated in the table caption.
[32] H. Song and J. J. Hoyt, Comput. Mater. Sci. **117**, 151 (2016).
[33] G. J. Ackland, D. J. Bacon, A. F. Calder, and T. Harry, Philos. Mag. A **75**, 713 (1997).
[34] S. Karewar, J. Sietsma, and M. J. Santofimia, Acta Mater. **142**, 71 (2018).
[35] I. Bleskov, T. Hickel, J. Neugebauer, and A. Ruban, Phys. Rev. B **93**, 214115 (2016).
[36] B. Wang, E. Sak-Saracino, N. Gunkelmann, and H. M. Urbassek, Comput. Mater. Sci. **82**, 399 (2014).
[37] J. Meiser and H. M. Urbassek, AIP Adv. **6**, 085017 (2016).
[38] J. W. Cahn, Acta Metallurgica **5**, 169 (1957).
[39] C. C. Dollins, Acta Metallurgica **18**, 1209 (1970).
[40] Y. Gao, C. J. Ruestes, D. R. Tramontina, and H. M. Urbassek, J. Mech. Phys. Sol. **75**, 58 (2015).
[41] C. J. Ruestes, E. M. Bringa, Y. Gao, and H. M. Urbassek, in *Applied Nanoindentation in Advanced Materials*, edited by A. Tiwari and S. Natarajan (Wiley, Chichester, UK, 2017), chap. 14, pp. 313–345.